Cutting Tool Temperatures in Contour Turning: Transient Analysis and Experimental Verification

D. A. Stephenson
GM Powertrain Group Headquarters,
895 Joslyn Ave. MC2AE6,
Pontiac, MI 48340

T.-C. Jen
Mechanical Engineering Department,
University of Wisconsin, Milwaukee,
Milwaukee, WI 53201

A. S. Lavine
Mechanical and Aerospace
Engineering Department,
University of California,
Los Angeles, CA 90095-1597

This paper describes a model for predicting cutting tool temperatures under transient conditions. It is applicable to processes such as contour turning, in which the cutting speed, feed rate, and depth of cut may vary continuously with time. The model is intended for use in process development and trouble shooting. Therefore, emphasis is given in the model development to enable rapid computation and to avoid the need to specify parameters such as thermal contact resistances and convection coefficients which are not known in practice. Experiments were conducted to validate the predictive model. The model predictions with two different boundary conditions bound the experimental results. An example is presented which shows the utility of the model for process planning.

1 Introduction

In machining operations, mechanical work is converted to heat through the plastic deformation involved in chip formation and through friction between the tool and workpiece. Some of this heat conducts into the cutting tool, resulting in high tool temperatures near the cutting edge. Elevated tool temperatures have a negative impact on tool life. Tools become softer and wear more rapidly by abrasion as temperatures are increased, and in many cases constituents of the tool may diffuse into the chip or react chemically with the workpiece or cutting fluid.

Because of their impact on tool life, cutting temperatures have been widely studied for many years. Most research, however, has been restricted to steady-state temperatures in relatively simple processes, such as orthogonal cutting or cylindrical turning, in which the cutting speed, feed rate, and depth of cut are constant (Trigger and Chao, 1951; Barrow, 1973; Shaw, 1984; Boothroyd and Knight, 1989; Strenkowski and Moon, 1990; Stephenson, 1991; Chandra and Chen, 1994). In most industrial machining processes, however, these parameters vary with time, so that a steady-state temperature field is never established.

Recently, transient cutting temperatures have been investigated for interrupted turning, a process in which the cutting speed, depth of cut, and feed rate remain constant, but in which the tool periodically enters and exits the workpiece, so that the heat input to the tool is periodic. Stephenson and Ali (1992) used a Green's function approach to calculate tool temperatures in interrupted cutting. Their results agreed reasonably well with experimental data. However, they assumed the tool to be semi-infinite in all directions; this is an adequate approximation for interrupted cutting, in which heating times are on the order of 10 ms, but is probably not adequate for contour turning, in which heating times are typically between 10 and 60 seconds. Radulescu and Kapoor (1994) used the separation of variables method to solve the same problem for a finite tool (and the corresponding temperature distributions in the workpiece and chip). Their results also agreed well with experiments, but they used convection boundary conditions at the boundaries exposed to the environment, which increase computing times and introduce inputs which are difficult to specify in practice.

A more practically important process in which the temperature response is transient is contour turning (Fig. 1), a process for producing complex axisymmetric parts from castings or forgings. In this process the cutting action is generally continuous, but the cutting speed, depth of cut, and feed rate may all vary with time. This results in temporal variations in both the magnitude of the heat input to the tool and the area of the tool over which heat is input. Currently, the common practice for extending tool life in contour turning is to vary the spindle speed as the radius being cut varies so that the peripheral speed remains constant, in an attempt to keep cutting temperatures constant. Variations in the depth of cut and feed rate, however, still lead to increases in cutting temperatures and wear rates over portions of the cut, which reduces tool life.

This paper describes a method for calculating cutting tool temperatures in contour turning. The analysis, described in Section 2, builds on Radulescu and Kapoor's (1994) model for temperatures in interrupted cutting. The model is adapted to account for variations in dimensions of the heat source with time. In addition, insulated conditions are used on the boundaries exposed to the environment, to simplify input requirements and reduce computing times. Finally, either insulated or ambient temperature boundary conditions are used at the bottom surface of the tool insert, to roughly bound the true solution. With these changes, the model is suitable for use in workstation-based process simulations. Measurements of cutting temperatures in simple contour turning experiments are described in Section 3. Two types of experiments were conducted: facing cuts in which the cutting speed is varied while the feed rate and depth of cut remain constant, and step cutting experiments in which all parameters remain constant except the depth of cut, which undergoes a step change. These experiments are designed to simulate two basic types of contouring cuts: facing cuts and OD cuts. Measured and calculated temperatures are compared and shown to agree well in Section 4. Calculations for a sample part which show how the results can be used to identify areas where peak temperatures and wear rates can be expected to occur are described in Section 5.

2 Analysis

The purpose of the present study was to develop a simulation program to calculate cutting tool temperatures which would be

Contributed by the Manufacturing Engineering Division for publication in the JOURNAL OF MANUFACTURING SCIENCE AND ENGINEERING. Manuscript received May 1995; revised May 1996. Associate Technical Editor: M. Elbestawi.

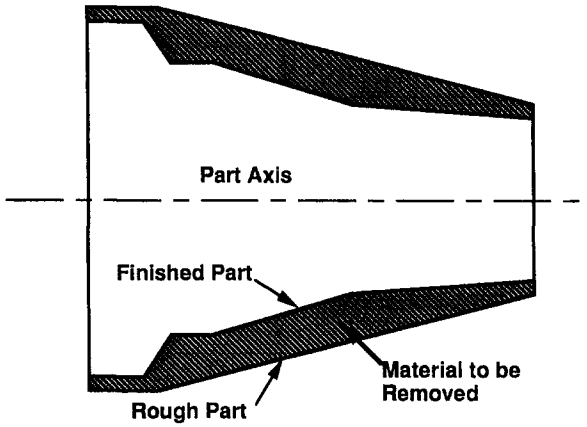

Fig. 1 Contour turning

useful in an industrial setting for process development. The requirements therefore were that the simulation run reasonably quickly and that the inputs to the model be known or easily determined quantities. These requirements affected the choice of an algorithm for calculating the tool temperature, as described below.

Consider a cutting tool with a rectangular tool insert, cutting into the workpiece (Fig. 2). There is a heat source in the corner of one face of the tool insert, where it comes in contact with the chip. To solve for the tool temperature distribution, a computational domain must be selected, and appropriate boundary conditions must be specified. As the cutting process progresses, the heat entering the tool at the tool-chip interface penetrates further into the tool. Ideally, the computational domain should be chosen to be larger than the depth to which there is significant heat penetration. However, this depth is not known a priori. Furthermore, if the computational domain is chosen to be larger than the tool insert, then the thermal contact resistance at the insert-holder interface must be known in order to completely specify the problem. Unfortunately, this contact resistance is typically not well-known, and depends on the particulars of the surface roughness of the interfaces and how the insert is clamped into the holder. To avoid the need to specify the contact resistance, the following approach was taken. The computational domain was selected to be the same size as the tool insert, and approximate boundary conditions were specified at the tool-holder interfaces, as described in the next paragraph.

The tool insert has three of its boundaries in contact with the holder (at $x = d$, $y = e$, and $z = f$), which will be called the "interior boundaries." In Radulescu and Kapoor's (1994) approach, these boundaries were assumed to be at the ambient temperature. In Stephenson and Ali's (1992) work, these boundaries were assumed to be at infinity (and therefore at the ambient temperature). These assumed boundary conditions yielded temperatures at the tool-chip interface which were in reasonable agreement with measurements, for a particular set of conditions. However, under a different set of conditions (Stephenson, 1993), experiments indicated that the temperature at the bottom surface of the insert ($z = f$) in Fig. 2 could be as high as 200°C. Therefore, for this boundary, two types of thermal boundary condition were considered which bound the actual situation: (a) ambient temperature, and (b) insulated surface. The insulated boundary condition will yield higher calculated temperatures than the ambient temperature boundary condition; we expected actual (measured) temperatures to fall between the temperatures calculated for the two cases. For the other two interior boundaries, which are farther from the heat source, only the ambient temperature boundary condition was used.

The other three boundaries of the tool insert (at $x = 0$, $y = 0$, and $z = 0$) are exposed to the environment (except where the tool is in contact with the chip). These will be called the "exterior boundaries." Many production processes, especially those in which ceramic tools are used, are carried out dry (without coolant). If no coolant is used, the heat transfer to the air is typically negligible relative to the heat entering the tool (Jen and Lavine, 1994), and so the exterior boundaries are assumed insulated. This assumption is not as accurate for operations in which a water-based coolant is used. In this case the temperature at the tool-chip interface (near the heat source) would be slightly lower (by roughly ten percent; Li et al., 1995), although the temperature field away from the contact would be more significantly affected. The solution could be extended to account for convection at the exterior boundaries in the manner described by Radulescu and Kapoor (1994). This would require specification of surface heat transfer coefficients, which are generally not known in practice. Machining with oil-based lubricants can be simulated using insulated boundary conditions by adjusting the heat source strength to reflect reduced friction.

With this background, the problem can now be solved. The three-dimensional, transient heat conduction equation, assuming constant thermal properties, is:

$$\frac{1}{\alpha_T}\frac{\partial T}{\partial t} = \frac{\partial^2 T}{\partial x^2} + \frac{\partial^2 T}{\partial y^2} + \frac{\partial^2 T}{\partial z^2} + \frac{\dot{q}(x, y, z, t)}{k_T} \tag{1}$$

where k_T and α_T are the tool thermal conductivity and thermal diffusivity, respectively. The heat source term, $\dot{q}(x, y, z, t)$, will be treated as a spatially uniform plane heat source on the surface of the insert (Radulescu and Kapoor, 1994), expressed as follows:

$$\dot{q}(x,y,z,t) = \begin{cases} q(t)\cdot\delta(z) & 0 \le x \le L_x;\quad 0 \le y \le L_y \\ 0 & \text{otherwise} \end{cases} \tag{2}$$

Here, $\delta(z)$ is the Dirac delta function and $q(t)$ is the heat flux entering the tool through the darkened region in Fig. 2 in the corner of one surface, which is the contact area between the cutting tool and the chip (assumed rectangular even though it is not in reality). In the analysis to be presented, the heat flux and contact area are assumed to be known functions of time. The contact area is determined from experimental measurements described in the next section. The heat flux is determined from measured cutting forces using Loewen and Shaw's model (1954). This model is also used for determining the approximate tool-chip interface temperature at which to evaluate the thermal properties at each time step. The initial and boundary conditions are:

$$T(x, y, z, 0) = T_0 \tag{3}$$

$$\left.\frac{\partial T}{\partial x}\right|_{x=0} = \left.\frac{\partial T}{\partial y}\right|_{y=0} = \left.\frac{\partial T}{\partial z}\right|_{z=0} = 0 \tag{4}$$

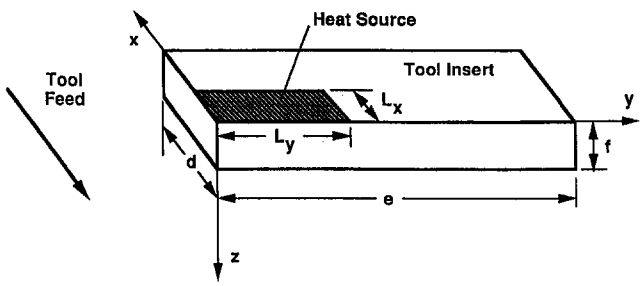

Fig. 2 Computational domain

and

$$T(d, y, z, t) = T(x, e, z, t) = T_0 \tag{5}$$

and either

$$T(x, y, f, t) = T_0 \tag{6}$$

for the bottom surface at the ambient temperature, or

$$\left.\frac{\partial T}{\partial z}\right|_{z=f} = 0 \tag{7}$$

for an insulated bottom surface.

The solution is determined using separation of variables as in Radulescu and Kapoor (1994). The series solution can be expressed as follows:

$$\theta(x, y, z, t) = T(x, y, z, t) - T_0 = \sum_{i=0}^{\infty}\sum_{j=0}^{\infty}\sum_{k=0}^{\infty} \Theta_{ijk} \cdot \cos\, \alpha_i x \cdot \cos\, \beta_j y \cdot \cos\, \gamma_k z \tag{8}$$

where

$$\alpha_i \cdot d = \frac{2i + 1}{2}\pi, \quad \beta_j \cdot e = \frac{2j + 1}{2}\pi \tag{9}$$

and γ_k depends on the choice of boundary condition:

$$\gamma_k \cdot f = \frac{2k + 1}{2}\pi \tag{10}$$

for bottom surface at the ambient temperature, or

$$\gamma_k \cdot f = k\pi \tag{11}$$

for an insulated bottom surface.

The functions $\Theta_{ijk}(t)$ are calculated such that the governing differential equation and the initial condition are satisfied:

$$\frac{d\Theta_{ijk}}{dt} + \omega_{ijk}\Theta_{ijk} = \Omega_{ijk}(t) \tag{12}$$

and $\Theta_{ijk}(0) = 0$ where

$$\omega_{ijk} = \alpha_T(\alpha_i^2 + \beta_j^2 + \gamma_k^2) \tag{13}$$

and

$$\Omega_{ijk} = \left[\frac{8\alpha_T}{k_T def'} \cdot \frac{\sin\, \alpha_i L_x}{\alpha_i} \cdot \frac{\sin\, \beta_j L_y}{\beta_j}\right] q(t) \tag{14}$$

where $f' = f$ except for when the index k is zero in the case of an insulated bottom surface; then $f' = 2f$.

An analytical solution can be found for $\Theta_{ijk}(t)$, provided that the time dependence of $q(t)$ is sufficiently simple. In particular, when the heat flux comes from experimental data taken at discrete time intervals (as it does in the present paper), it is particularly natural to approximate it by a piecewise constant function, i.e., $q(t) \approx q_p$ for $\tau_{p-1} < t < \tau_p$. Then the solution is (where the p subscript on any quantity implies its value in the time period $\tau_{p-1} < t < \tau_p$):

$$\Theta_{ijk,1}(t) = -\frac{\Omega_{ijk,1}}{\omega_{ijk}}\left[e^{-\omega_{ijk}t} - 1\right] \tag{15}$$

$$\Theta_{ijk,p}(t) = \left[\Theta_{ijk,p-1}(\tau_{p-1}) - \frac{\Omega_{ijk,p}}{\omega_{ijk}}\right] \cdot e^{-\omega_{ijk}(t-\tau_{p-1})} + \frac{\Omega_{ijk,p}}{\omega_{ijk}} \tag{16}$$

where $p = 2, 3, \ldots$ in Eq. (16).

Once the solution is determined, the average tool-chip temperature can be found by integrating the temperature over the heat source area:

$$\theta_{ave}(t) = \frac{1}{L_x \cdot L_y}\int_0^{L_y}\int_0^{L_x} \theta(x, y, 0, t) \cdot dx \cdot dy = \frac{1}{L_x \cdot L_y}\sum_{i=0}^{\infty}\sum_{j=0}^{\infty}\sum_{k=0}^{\infty} \Theta_{ijk}(t) \cdot \frac{\sin\, \alpha_i L_x}{\alpha_i} \cdot \frac{\sin\, \beta_j L_y}{\beta_j} \tag{17}$$

Series convergence tests have been performed for typical cases by comparing solutions of Eq. (17) for 100 × 100 × 100 terms and 120 × 120 × 120 terms. The difference between the two solutions, normalized by the temperature rise relative to the ambient, was less than 2 percent during the initial transient, and less than 0.5 percent at larger times. Thus, 100 × 100 × 100 terms is considered sufficient, and is used throughout the present study. Unfortunately, each term in the series contains an exponential (Eq. 16), which is relatively time-consuming to compute. There are a number of ways to reduce the computational time. We chose to use a power law approximation (Patankar, 1980) for the exponential terms, which reduces the total computational time by a factor of six or seven. The approximation replaces $e^{-\lambda}$ with $f(\lambda)$, where:

$$f(\lambda) = \begin{cases} \dfrac{(1 - 0.1 \cdot \lambda)^5}{\lambda + (1 - 0.1 \cdot \lambda)^5} & 0 \le \lambda \le 10 \\ 0 & \lambda > 10 \end{cases} \tag{18}$$

The absolute error in $f(\lambda)$ is less than 0.0055 for all λ. For a typical computation of average tool-chip temperature, the error is less than 0.5 percent. Alternatively, the summation routine could have been written so that the terms in Eq. (16) involving exponentials were truncated earlier than the non-exponential terms.

The average tool-chip temperature predicted by the analysis will be compared with experimental data, and the effect of the two types of boundary conditions assumed at the bottom surface will be discussed.

3 Experiments

Average tool-chip interface temperatures calculated using the analysis described in the previous section were compared to measured temperatures from two types of experiments. In the first type (Fig. 3), a facing cut was performed on a solid cylinder at a constant spindle rpm, radial feed rate, and axial depth of cut. The area of cut remained constant with time, but the cutting speed and thus the rate of heat generation at the tool-chip interface decreased linearly with the radius being cut. We expected the force to remain constant and the cutting temperature to decrease with time. This experiment simulates facing cuts on flange or thrust surfaces. In the second type of experi-

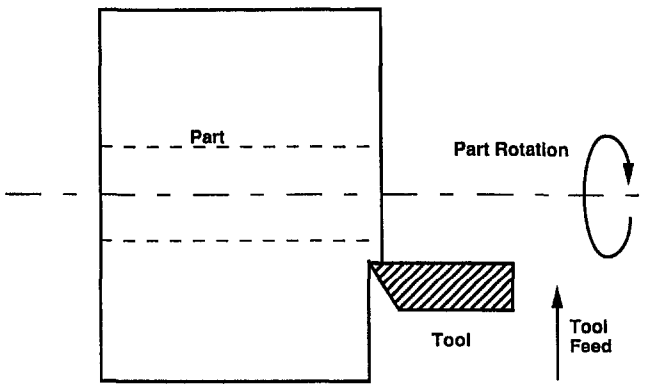

Fig. 3 Face cutting experiment

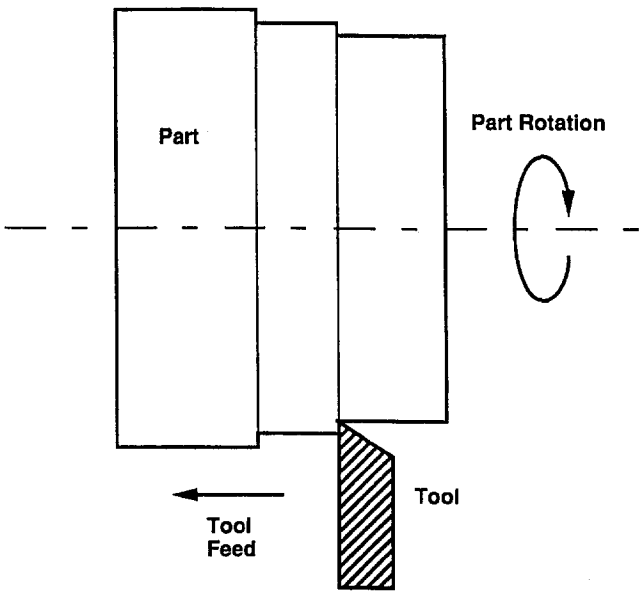

Fig. 4 Step cutting experiment

ment (Fig. 4), an OD cut was performed at a constant spindle speed and axial feed rate on a part having a step change in diameter. The cutting speed remained constant while the depth and thus the area of cut underwent a step increase in the middle of the cut. We expected the cutting temperature to remain constant while the cutting force underwent a step increase with time. This experiment simulates an OD cut on a bearing surface with a varying depth of cut.

Two materials were cut: cold drawn 1018 steel and 2024-T6 aluminum. For both materials, specimens were cut from a single billet of cold worked stock to minimize variations in material properties. Uncoated C2 grade Tungsten Carbide tools ground from 105-mm long reamer blanks were used. This tool geometry and special bakelite tool holders were used to reduce temperature measurement errors (Stephenson, 1991). The tools had side rake, back rake, and lead angles of −5 deg, 0 deg, and 10 deg, respectively. The final tool dimensions were $d = 8.3$ mm, $e = 102$ mm, $f = 2.65$ mm. Cutting conditions for all tests are summarized in Table 1. All work samples cut had an initial outside diameter of 190 mm; a 25.4 mm hole was drilled in the center of the specimens used in the facing tests so that the tool would not cut material at very low speeds near the center. The spindle speeds were chosen to prevent the formation of a built-up edge (BUE) on the tool and to produce average interfacial temperatures which were significantly below the melting temperature of the work material. For the aluminum work material, the speed was kept above 50 m/min to prevent BUE formation, but below 400 m/min to prevent melting of the chip. These speed limits were identified in initial trial cuts. All tests were replicated to ensure that repeatable results were being obtained.

Quantities measured in the tests included the cutting forces, average tool-chip temperature θ_{ave}, and the chip thickness and tool-chip contact length L_x. Cutting forces were measured using a piezoelectric dynamometer. The average interfacial temperature was measured using the tool-work thermocouple method. The thermocouple circuit was insulated from the machine tool using a bakelite tool holder and calibrated using the torch method as described in previous papers (Stephenson, 1991 and 1993). A lead angle of 10 deg was used in all tests to guide the chip away from the machined surface to prevent short circuiting of the tool-chip thermocouple circuit. The chip thickness was measured using a point micrometer and the tool-chip contact length was measured using the wear scar method (Stephenson, 1989). Both these parameters varied with the cutting speed; the variation was characterized by curve-fitting measurements taken at 1.25 cm radial intervals during the facing cuts. The variations were well represented by the equations:

$$t_2 = \begin{cases} 1.307 \cdot V^{-0.256} & \text{(Al 2024)} \\ 0.258 + 0.00285 \cdot V & \text{(1018 steel)} \end{cases} \quad (19)$$

$$L_c = \begin{cases} 2.421 \cdot V^{-0.294} & \text{(Al 2024)} \\ 0.485 + 0.00280 \cdot V & \text{(1018 steel)} \end{cases} \quad (20)$$

where t_2 and L_c are the chip thickness and tool-chip contact length in mm and V is the cutting speed in m/min.

4 Comparison Between Experiments and Calculations

The tool-chip average temperature was calculated for conditions corresponding to the experiments described in the preceding section. The needed inputs to the thermal model are: (1) dimensions: d, e, and f from the actual insert geometry as specified in the previous section; $L_x = L_c$ from Eq. (20) using V from Table 1; L_y = depth of cut from Table 1. (2) thermal properties: the temperature dependence of k_T and α_T for the materials in question is documented in Stephenson (1991). Following the successful approach used by Stephenson and Ali (1992), the values used in the calculations were those corresponding to the instantaneous tool-chip temperature predicted by Loewen and Shaw's (1954) model. (3) heat flux $q(t)$: from Loewen and Shaw's model using the information in Table 1, along with t_2 and L_c from Eqs. (19) and (20), and the measured cutting forces. Figures 5–10 illustrate the temperatures as a function of time for each of the tests. The symbols are the experimental data and the two lines are the calculations with the two different boundary conditions at the bottom surface of the insert. The results are consistent with the expected variations in cutting temperature with time for the step and face cutting tests; the temperature is roughly constant in time for the step cutting tests (Figs. 7 and 10), but decreases steadily with time for the face cutting tests (Figs. 5, 6, 8, and 9).

The observed rapid variations in the measured tool-chip thermocouple signals were investigated in Stephenson (1993). It was found that they are caused by two physical phenomena. First, when long, continuous chips are formed, the chip may strike the workpiece at a point away from the tool, producing contact at a low-temperature junction which essentially grounds

Table 1 Cutting conditions used in the facing and step cutting tests

	1018 Steel			2024-T6 Aluminum		
	Face Cutting		Step Cutting	Face Cutting		Step Cutting
Case	1	2	3	4	5	6
spindle speed (rpm)	102	137	102	610	1000	610
min. cutting speed (m/min)	8.1	10.9	61.5	48.7	79.8	365.1
max. cutting speed (m/min)	61.5	82.0	61.5	365.1	598.5	365.1
feed rate (mm/rev)	0.127	0.127	0.127	0.165	0.165	0.165
depth of cut (mm)	0.762	0.762	0.381 to 0.762	1.905	1.905	0.635 to 1.270

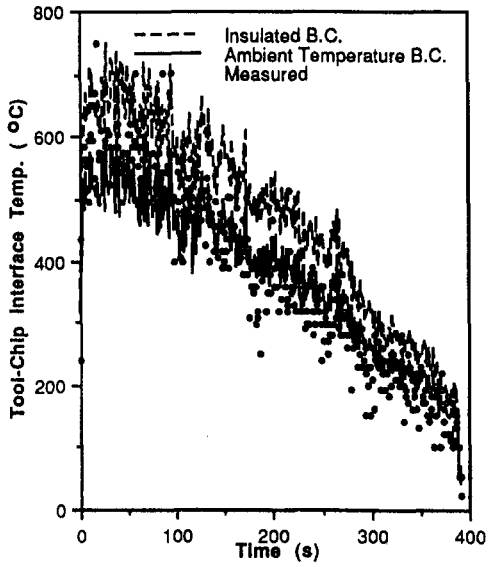

Fig. 5 Comparison of calculated and measured average tool-chip interface temperatures for case 1

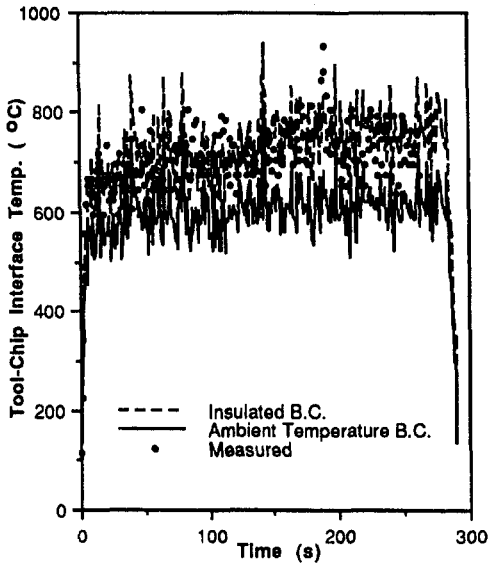

Fig. 7 Comparison of calculated and measured average tool-chip interface temperatures for case 3

the circuit. This leads to intervals of zero voltage in the signal. Under constant cutting conditions this problem can be avoided by choosing a tool geometry which properly directs chip flow. Under varying conditions, however, the chip flow direction changes with time, making this solution difficult to apply. This was a more serious problem when cutting the steel samples in the present experiments. A second source of variation in the measured signals was the periodic growth and breakage of the chip, which is particularly pronounced when cutting materials such as 2024 Al which form short, tightly curled chips which break due to periodic contact with the workpiece. This can result in both short circuiting and in periods in which the tool-chip circuit is open due to loss of contact between the tool and chip, and produces periodic variations in the measured signal which depend to some extent on the open-circuit behavior of the circuit amplifier. The large variations in the measured signal in Fig. 10 result from this source. The magnitude of the variations in the measured signals, which is often equal to the difference in temperature for the solutions with insulated and ambient temperature boundary conditions, indicate that the use of more complex boundary conditions (e.g., a thermal contact resistance boundary condition) would not lead to a verifiable increase in accuracy. The smaller, but still pronounced, variation in the model predictions comes from variation in the measured forces.

The choice of boundary condition at the bottom of the insert affects the tool-chip temperature significantly: the difference between the two cases can be as much as 200°C. This difference develops within the first ten seconds of the cutting process, indicating that there is significant thermal penetration to the bottom of the insert even at these early times. It is clearly worth some effort to provide good thermal contact between the insert and the holder in practice, as it has the potential to lower the tool temperature significantly.

As expected, the two analytical solutions generally act as upper and lower bounds to the measured temperature signal. For the steel cases (Figs. 5 through 7), neither solution provides a significantly better fit to the experimental data. In process planning work, the insulated boundary condition should be used,

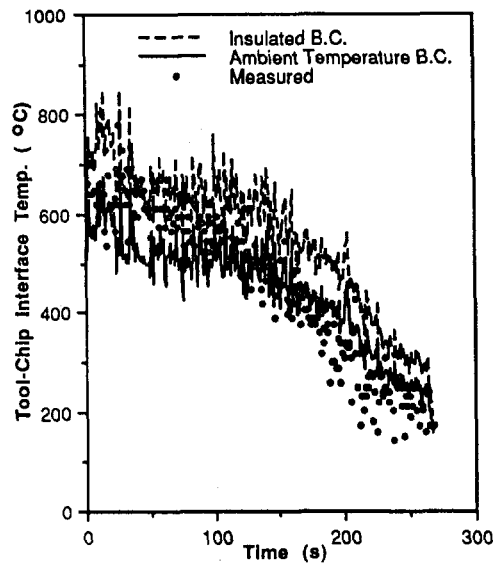

Fig. 6 Comparison of calculated and measured average tool-chip interface temperatures for case 2

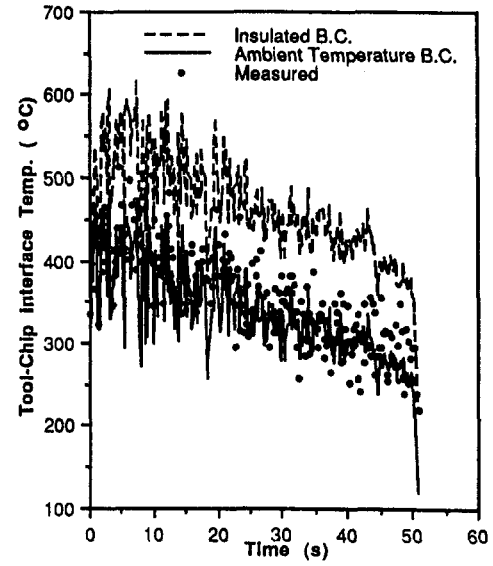

Fig. 8 Comparison of calculated and measured average tool-chip interface temperatures for case 4

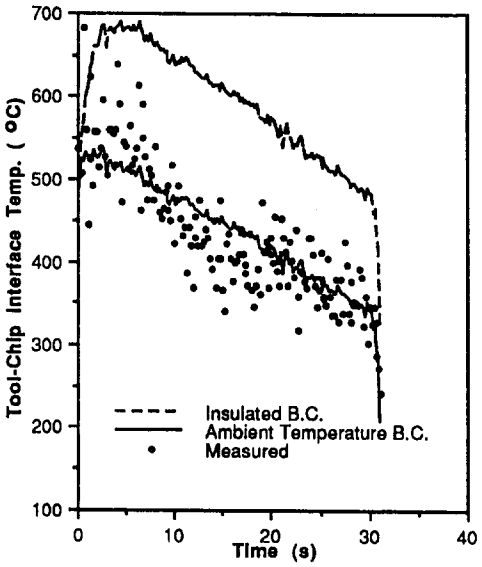

Fig. 9 Comparison of calculated and measured average tool-chip interface temperatures for case 5

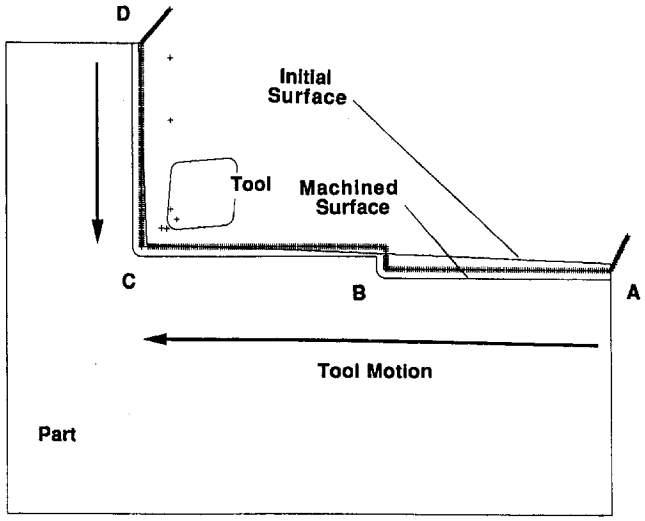

Fig. 11 Part geometry and tool path for machining a part with a bearing surface, shoulder, and flange. The tool moves from points A to B to C, and is then withdrawn and machines from points D to C.

as this will provide conservative temperature estimates. In the aluminum cases (Figs. 8 through 10), the experimental data agrees better with the solution for the ambient temperature boundary condition. This is surprising because contact resistance between the (carbide) tool and (bakelite) holder used in the experiments would be expected to be high, and would be expected to be better represented by an insulated boundary condition. Possible explanations for this result include systematic errors in calculating the heat input to the tool and inaccuracies in the thermoelectric calibration used to convert measured emf's to temperatures. The heat input to the tool was calculated using Loewen and Shaw's (1954) model for steady state temperatures, which has been shown to be more accurate for materials like 1018 steel, which form long, continuous chips, than for materials such as 2024 aluminum, which form short, tightly curled chips (Stephenson, 1991). Accurate thermoelectric calibration is more difficult for aluminum alloys than for steels, since nonferrous alloys with relatively low melting points exhibit a thermoelectric hysteresis effect and yield different calibration curves when subjected to repeated heating and cooling cycles (Byrne, 1987). Accurate temperature calculations are of more practical interest for steels than for aluminum alloys. As with the steel, using the insulated boundary condition for process planning calculations with the aluminum would yield conservative temperature estimates.

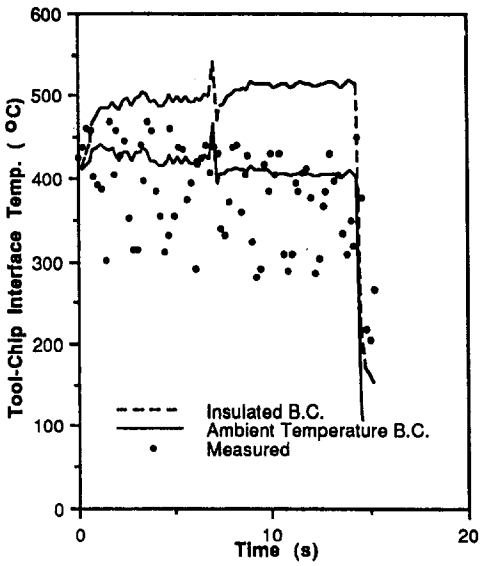

Fig. 10 Comparison of calculated and measured average tool-chip interface temperatures for case 6

5 Example Application

As an example of how the temperature model described in this paper can be applied, the turning of the part shown in Fig. 11 can be considered. This part has features typical of mass produced rotational parts including constant diameter bearing surfaces (A to B and B to C), a locating shoulder (at point B), and a flange for locating or mounting (D to C). Figure 11 shows the uncut and finished part profile and the tool path (+ symbols) drawn by a commercial CAM system. Note that there are regions in which the tool does not contact the workpiece (when the + symbols are outside of the initial surface). The depth of cut varies up to 3.0 mm. The workpiece was taken to be medium carbon steel and the tool to be a CNMG-544 aluminum oxide coated WC insert.

Forces for machining this part were calculated using an analysis similar to that described by Kuhl (1987). In this approach, the area of material being cut at any time, C_{area}, is calculated from geometric considerations. The average uncut thickness of this area t_{ave} (i.e., the thickness of an equivalent contact rectangular contact area) is determined from the feed rate, depth of cut, tool nose radius, and tool lead angle. The cutting forces are then calculated as exponential functions of this thickness:

$$F = C_{\text{area}} \cdot K \cdot t_{\text{ave}}^{b} \tag{21}$$

Separate equations are used for the force normal and parallel to the tool face. The constants K and b are fit from experimental data; for the calculations in this paper, values typical of low carbon steel were used. In these calculations, it was also assumed that the deformed chip thickness was equal to 3 t_{ave}, and that the tool-chip contact length was equal to 5 t_{ave}. These assumptions were identified from previous data for machining steel with negative rake tools (Stephenson, 1989; Stephenson, 1991) and are consistent with Eqs. (18) and (19), although some thinning of the chip with increasing cutting speed would be expected.

The calculated variation of the tool-chip interface temperature with time when cutting at a constant surface speed of 200 m/

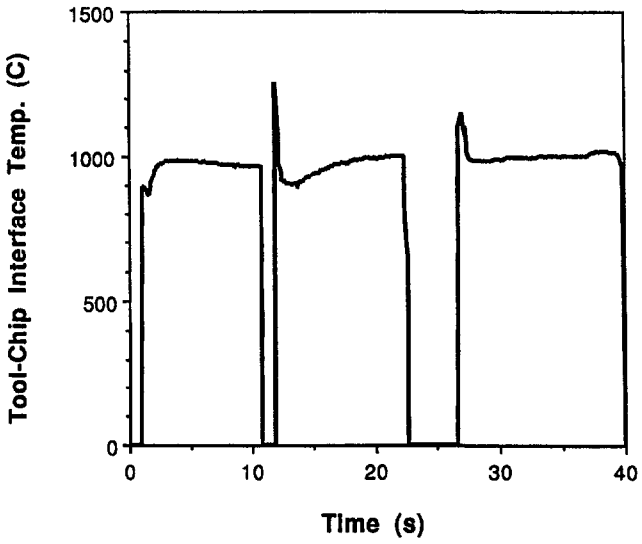

Fig. 12 Average tool-chip interface temperature for machining the part shown in Fig. 11 at a constant surface speed of 200 m/min and a constant feed rate of 0.4 mm/min.

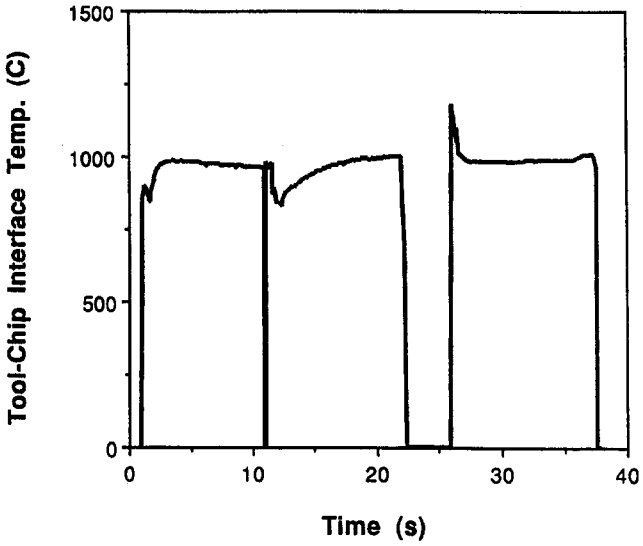

Fig. 14 Average tool-chip interface temperature for machining the part shown in Fig. 13. Speed and feed are 200 m/min and 0.4 mm/rev, respectively, for the bearing surfaces (point A to point C), and 180 m/min and 0.5 mm/rev for the flange surface (point D to C)

min and a constant feed rate 0.4 mm/rev is shown in Fig. 12 (assuming an insulated boundary condition at the bottom surface). During the time periods when the tool does not contact the workpiece, the concept of a "tool-chip interface temperature" is meaningless, and the temperature was arbitrarily set to zero on the figure. Note that although the surface speed is constant, the temperature shows significant variation, primarily because t_{ave} and thus the ratio of the cutting force to the contact area (which determines the strength of the heat flux into the tool) varies. The highest computed temperatures occur at point B, since the tool exits the part when cutting the locating shoulder and then reenters, initially cutting a very thin chip. Since b in Eq. (21) is always negative, this leads to a high specific force, high heat flux, and high temperature over the nose of the tool at this point. Such "spikes" in temperature can result in excessive insert nose wear.

Based on the computed temperature results, two modifications were made to the process as illustrated in Fig. 13. First, a 2 mm radius was added to the part at point B to increase chip dimensions and reduce tool nose temperatures at this point.

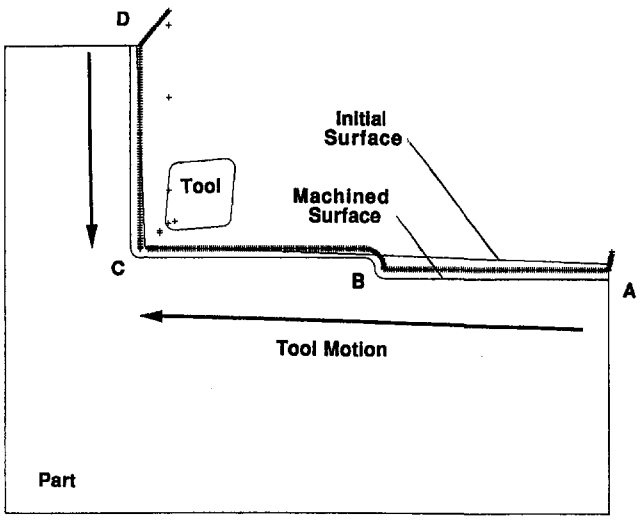

Fig. 13 Modification of the part shown in Fig. 11, incorporating a 2 mm radius at point B

Second, the cutting speed and feed rates were changed to 180 m/min and 0.5 mm/rev respectively on the flange surface (D to C). The second change was made to reduce the cutting time while maintaining a constant tool temperature; increasing the feed increases the roughness of the machined surface, but surface finish is generally not critical on flanges. The computed tool temperature profile for the modified tool path is shown in Fig. 14. Note that the magnitude of the temperature increase at point B has been significantly reduced (by roughly 100°C), which should reduce insert nose wear, and that the change in speed and feed on the flange face has resulted in a 10 percent reduction in the total cycle time without increasing the tool temperature. Further improvements could be made by modifying the incoming part profile or the tool geometry.

6 Summary and Conclusion

This paper describes a model for calculating cutting tool temperatures under transient conditions, with time varying heat flux and tool-chip contact area. The model is based on an analytical solution for the temperature in a rectangular insert subjected to a piecewise constant heat flux. Calculated temperatures are compared to measured temperatures from face- and step-cutting tests on steel and aluminum workpieces. Calculations for two boundary conditions for the bottom surface of the insert provide upper and lower bounds when compared to the measurements, with the lower bound solution (assuming an ambient temperature boundary condition) generally agreeing well with the data. An example application is presented which shows how the model can be used in process planning to reduce peak tool temperatures and cycle times.

Acknowledgments

TJ and AL thank the National Science Foundation for their support of the analytical portion of this work. We are also grateful to Kishor Patel for his assistance in carrying out some of the calculations.

References

Barrow, G., 1973, "A Review of Experimental and Theoretical Techniques for Assessing Cutting Temperatures," *CIRP Annals*, Vol. 22, pp. 203–211.

Boothroyd, G., and Knight, W. A., 1989, *Fundamentals of Machining and Machine Tools*, Marcel Dekker, New York, Chap. 3.

Byrne, G., 1987, "Thermoelectric Signal Characteristics and Average Interfacial Temperatures in the Machining of Metals Under Geometrically Defined Conditions," *Int. J. Machine Tools Manuf.,* Vol. 27, pp. 215–224.

Chandra, A., and Chan, C. L., 1994, "Thermal Aspects of Machining: A BEM Approach," *Int. J. Solids. Struct.,* Vol. 31, pp. 1657–1693.

Jen, T. C., and Lavine, A. S., 1994, "Prediction of Tool Temperatures in Interrupted Metal Cutting," *Proc. of 7th Int'l. Symposium on Transport Phenomena in Manufacturing Processes,* pp. 211–216.

Kuhl, M. J., 1987, "The Prediction of Cutting Forces and Surface Accuracy for the Turning Process," M.S. Thesis, Mechanical Engineering, University of Illinois.

Li, X., Kopalinsky, B. E., and Oxley, P. L. B., 1995, "A Numerical Method for Determining Temperature Distributions in Machining with Coolant, Parts 1 and 2," *Proc. Inst. Mech. Eng.,* Series B, Vol. 209, 33–52.

Loewen, E. G., and Shaw, M. C., 1954, "On the Analysis of Cutting Tool Temperatures," *Transactions of the ASME,* Vol. 76, pp. 217–231.

Patankar, S. V., 1980, *Numerical Heat Transfer and Fluid Flow,* Hemisphere Publishing Co., pp. 96–100.

Radulescu, R., and Kapoor, S. G., 1994, "An Analytical Model for Prediction of Tool Temperature Fields during Continuous and Interrupted Cutting," ASME *Journal of Engineering for Industry,* Vol. 116, pp. 135–143.

Shaw, M. C., 1984, *Metal Cutting Principles,* Oxford University Press, Oxford, Chap. 12.

Stephenson, D. A., 1989, "Material Characterization for Metal Cutting Force Modeling," ASME *Journal of Engineering Materials and Technology,* Vol. 111, pp. 210–219.

Stephenson, D. A., 1991, "Assessment of Steady-State Metal Cutting Temperature Models Based on Simultaneous Infrared and Thermocouple Data," ASME *Journal of Engineering for Industry,* Vol. 113, pp. 121–128.

Stephenson, D. A., and Ali, A., 1992, "Tool Temperature in Interrupted Metal Cutting," ASME *Journal of Engineering for Industry,* Vol. 114, pp. 127–136.

Stephenson, D. A., 1993, "Tool-Work Thermocouple Temperature Measurements: Theory and Implementation Issues," ASME *Journal of Engineering for Industry,* Vol. 115, pp. 432–437.

Strenkowski, J. S., and Moon, K. J., 1990, "Finite Element Prediction of Chip Geometry and Tool/Workpiece Temperature Distribution in Orthogonal Machining," ASME *Journal of Engineering for Industry,* Vol. 112, pp. 313–318.

Trigger, K. J., and Chao, B. T., 1951, "An Analytical Evaluation of Metal Cutting Temperatures," *Transactions of the ASME,* Vol. 73, pp. 57–68.